Computers, Materials & Continua CMC, vol.65, no.1, pp.109-123, 2020

Computational Analysis of the Oscillatory Mixed Convection Flow along a Horizontal Circular Cylinder in Thermally Stratified Medium

Zia Ullah[1], Muhammad Ashraf[1], Saqib Zia[2], Yuming Chu[3, 4], Ilyas Khan[5, *] and Kottakkaran Sooppy Nisar[6]

Abstract: The present work emphasizes the significance of oscillatory mixed convection stratified fluid and heat transfer characteristics at different stations of non-conducting horizontally circular cylinder in the presence of thermally stratified medium. To remove the difficulties in illustrating the coupled PDE's, the finite-difference scheme with efficient primitive-variable formulation is proposed to transform dimensionless equations. The numerical simulations of coupled non-dimensional equations are computed in terms velocity of fluid, temperature and magnetic field which are computed to examine the fluctuating components of skin friction, heat transfer and current density for various emerging parameters. The governing parameters namely, thermally stratification parameter S_t, mixed-convection parameter λ, Prandtl number Pr, magnetic force parameter ξ and magnetic-Prandtl number γ are displayed graphically at selected values for velocity and heat transfer mechanism. It is computed that heat transfer attains maximum amplitude and good variations in the presence of thermally stratified parameter at each position $\alpha = \pi/6$, $\alpha = \pi/3$ and $\alpha = \pi$ around the surface of non-conducting horizontally cylinder. The velocity of fluid attains certain height at station $\alpha = \pi/6$ for higher value of stratification parameter. It is also found that the temperature gradient decreases with stratification parameter S_t, but it increases after a certain distance Y from the cylinder. The novelty of the current work is that due to non-conducting phenomena the magnetic effects are strongly observed far from the surface but exact at the surface are zero for each position.

[1] Department of Mathematics, Faculty of Science, University of Sargodha, Sargodha, Pakistan.

[2] Department of Mathematics, COMSATS University Islamabad, Islamabad, 44000, Pakistan.

[3] Department of Mathematics, Huzhou University, Huzhou, 313000, China.

[4] Hunan Provincial Key Laboratory of Mathematical Modeling and Analysis in Engineering, Changsha University of Science & Technology, Changsha, 410114, China.

[5] Faculty of Mathematics and Statistics, Ton Duc Thang University, Ho Chi Minh, 72915, Vietnam.

[6] Department of Mathematics, College of Arts and Sciences, Prince Sattam bin Abdulaziz University, Wadi Aldawaser, 11991, Saudi Arabia.

[*] Corresponding Author: Ilyas Khan. Email: ilyaskhan@tdtu.edu.vn.

Received: 10 May 2020; Accepted: 26 June 2020.

Keywords: Mixed-convection, oscillatory stratified flow, non-conducting cylinder, thermal stratification, heat transfer.

Nomenclature

u, v	Velocity along xy-direction	m s^{-1}	
H_x, H_y	Magnetic velocities in xy-direction	(Tesla)	
ν	Kinematic-viscosity	m^2 s^{-1}	
σ	Electrical conductivity	s m^{-1}	
μ	Dynamic viscosity	kg m^{-1} s^{-1}	
ρ	Density	kg m^{-3}	
g	Gravitational-acceleration	m s^{-2}	
β	Thermal-expansion	K^{-1}	
ν_m	Magnetic-permeability	H m^{-1}	
α	Thermal-diffusivity	m^2 s^{-1}	
T	Fluid Temperature	(K)	
T_∞	Ambient-temperature (K)		
R_{e_L}	Renolds number		
G_{r_L}	Grashof number		
C_p	Specific-heat J kg^{-1} K^{-1}		
Greek Letters			
τ	Shearing stress (P a)		
ξ	Magnetic force number		
λ	Mixed convection number		
θ	Dimensionless temperature		
Pr	The Prandtl number		
γ	Magnetic Prandtl number		

1 Introduction

In theoretical and practical point of view, the analysis of MHD mixed convection flow with thermal stratification medium is very important in engineering and industrial environments. The fluid with thermally stratification is the deposition of layers which arises due to variations in temperature. Good applications in thermal stratification mechanism are refrigeration and air conditioning, closed containers, environmental heated walls chambers, petroleum industries, boundary layer controls, insulation of buildings and heat exchange between soil and atmosphere. Ali et al. [Ali and Hussain (2017)] presented the numerical and experimental phenomena on natural convection heat transfer along a heated plate in the presence of thermally stratification medium. Ashraf et al. [Ashraf, Ahmad and Chamkha (2019)] computed a computational mechanism of natural convection flow around a curved surface with exothermic catalytic chemical reaction. Ashraf et al. [Ashraf, Chamkha, Iqbal et al. (2016); Ashraf and Fatima (2018); Ashraf, Fatima and Gorla (2017); Ashraf, Iqbal, Ahmad et al. (2017)] have explored different heat transfer cases around magnetized shapes numerically. Ashraf et al. [Ashraf, Khan and Gorla (2019)] constructed boundary layer phenomena of natural convection flow by means of plume numerically. Recently, Ashraf et al. [Ashraf and Ullah (2020)] discussed oscillatory heat and fluid flow mechanism around the surface of horizontally non-conducting circular cylinder numerically. Deka et al. [Deka and Neog (2009)] illustrated the transient behavior of natural convection flow along an accelerated vertical plate immersed in thermally stratified medium. A heat transfer phenomena in magnetic nano-dispersion filled in cubical cavity to check numerical results for free-convection flow by applying magnetic field effects numerically by Dixit et al. [Dixit and Pattamatta (2020)]. Gireesha et al. [Gireesha, Venkatesh, Shashikumar et al. (2017)] proposed a numerical model on dusty-fluid around a stretched surface situated in thermally stratification porous medium with uniform heat source theoretically. They found an increase in temperature field due to increasing values of radiation parameter. The Burger's fluid flow

mechanism around stretched sheet in a thermally stratified medium with magnetohydrodynamics effects has been illustrated numerically by Hayat et al. [Hayat, Asad and Alsaedi (2016)]. A technical mechanism of mixed convection Oldroyd-B fluid in a doubly stratified medium with thermal radiation and chemical reaction has been computed in Hayat et al. [Hayat, Muhammad, Shehzad et al. (2015)]. Hayat et al. [Hayat, Saeed, Asad et al. (2016)] performed a physical problem on heat and mass transfer characteristics around stretching cylinder numerically. They noted that the temperature gradient is reduced due to stratification parameter. Hayat et al. [Hayat, Waqas, Khan et al. (2016); Hayat, Waqas, Shehzad et al. (2016)] developed a numerical mechanism of magnetohydrodynamic mixed convection flow of thixotropic nanomaterial and Burger's nanofluids in the presence of thermally stratified medium. Hussain et al. [Hussain and Raheem (2013)] performed a natural convection heat transfer mechanism over a plane wall in the presence of thermally stratified porous medium. Ishak et al. [Ishak, Nazar and Pop (2008)] studied the stable stratified medium effects on mixed convection boundary layer flow along a vertical surface numerically. The effect of thermally stratification on mixed convection flow of micro polar fluid over a stretching surface by taking thermal radiation effects has been explored analytically by Mahmoud et al. [Mahmoud and Waheed (2013)]. Makinde et al. [Makinde and Reddy (2019)] investigated a numerical simulation on electrically conducting peristaltic flow of Casson fluid in the presence of slip-velocity in a porous-channel numerically. They examined that the magnitude of pressure gradient reduced due to an increase in slip parameter. A generalized MHD flow and heat transfer model over an exponentially stretched sheet with thermally stratification effects has been studied in Mukhopadhyay [Mukhopadhyay (2013)]. The thermal boundary layer thickness decreases with the increasing stratification values. The physical mechanism on mixed convection flow around a stretched cylinder placed in thermally stratification medium has been examined numerically by Mukhopadhyay et al. [Mukhopandhyay and Ishak (2012)]. They obtained lower rate of heat transfer at the surface in thermally stratification medium compared to that of unsaturated medium. Rehman et al. [Rehman, Malik, Salahuddin et al. (2016)] considered a flow analysis with heat generation/absorption effects on mixed convection flow of Eyring-Powell fluid around a stretching cylinder in the presence of double stratified medium numerically. A buoyant mechanism on natural convection flow along a vertical surface in a thermally stratified medium with thermal and mass diffusion effects has been considered theoretically by Saha et al. [Saha and Hossain (2004)]. A free convection heat transfer phenomena around a rotating sphere within the thermal stratification medium has been proposed numerically by Saikrishnan [Saikrishnan (2010)]. The ambient thermally stratification is found to decrease the local buoyancy levels that reduces the velocities and increases the concentrations. Ullah et al. [Ullah, Ashraf and Rashad (2020)] discussed oscillatory heat and fluid flow mechanism around the surface of horizontally non-conducting circular cylinder numerically. Vasu et al. [Vasu, Reddy, Murthy et al. (2017)] analyzed the significance of non-linear temperature density and entropy generation on thermally stratified fluid flow along a vertical plate embedded in a porous medium with thermal dispersion effects numerically. Vyas et al. [Vyas, Mishra and Srivastava (2020)] used a non-intrusive diagnostic technique to develop a heat transfer problem with experimental investigation around a square cylinder confined in a rectangular channel. A physical phenomena of mixed convection flow of nano-fluid in the presence of thermal stratification along a vertical

surface has been presented by Yasin et al. [Yasin, Arifin, Nazar et al. (2013)]. Zhang et al. [Zhang, Yin, Yang et al. (2017)] used spatial and spectral entropies with low scaling ratio on multi-scale images to detect image seam carving. Zhang et al. [Zhang, Li, Wang et al. (2018)] performed an ensemble learning method to check reliability of wireless multimedia device with a series of new threats and challenges.

Taking idea form above literature review, it is addressed that the oscillatory mixed convection flow around a non-conducting horizontally circular-cylinder in thermally stratified medium has not been yet examined by any researcher. Taking idea from the following [Saha and Hossain (2004)], we obtained a numerical method for above oscillatory fluid flow phenomena around different stations of non-conducting horizontally cylinder under thermally stratified medium. We explore velocity of fluid, the fluid temperature and velocity of magnetic field which are computed to conclude oscillating quantities of skin friction, fluctuating heat transfer and oscillatory current density.

2 The governing model and flow geometry

Considering two dimensional boundary-layer fluid flow phenomena at different stations of non-conducting horizontally cylinder is considered. The Fig. 1 represents distance along the surface is x, the normal y-direction of the surface and the velocities u and v along the xy-direction. The H_x is magnetic field at the cylinder surface, H_y is taking normal to the cylinder surface, the wall temperature is T_w and $T_{\infty,x}$ is ambient fluid temperature and external fluid velocity is $U(x,t)$. Moreover, magnetic field intensity proceeds along the normal direction of non-conducting horizontally cylinder surface. The dimensionlized boundary-layer equations are given below:

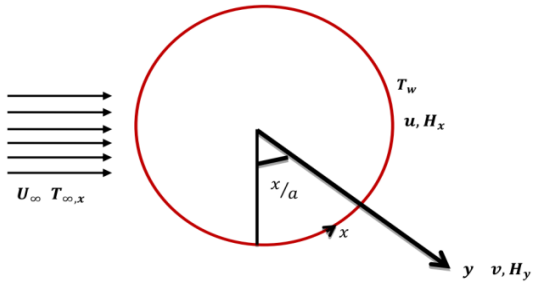

Figure 1: Non-conducting cylinder and flow geometry

$$\frac{\partial \bar{u}}{\partial \bar{x}} + \frac{\partial \bar{v}}{\partial \bar{y}} = 0 \tag{1}$$

$$\frac{\partial \bar{u}}{\partial \tau} + \bar{u}\frac{\partial \bar{u}}{\partial \bar{x}} + \bar{v}\frac{\partial \bar{u}}{\partial \bar{y}} = \frac{\partial^2 \bar{u}}{\partial \bar{y}^2} + \xi\left(\bar{h}_x \frac{\partial \bar{h}_x}{\partial \bar{y}} + \bar{h}_y \frac{\partial \bar{h}_x}{\partial \bar{y}}\right) + \lambda\bar{\theta}sin\alpha \tag{2}$$

$$\frac{\partial \bar{h}_x}{\partial \bar{x}} + \frac{\partial \bar{h}_y}{\partial \bar{y}} = 0 \tag{3}$$

$$\frac{\partial \bar{h}}{\partial \tau} + \bar{u}\frac{\partial \bar{h}}{\partial \bar{x}} + \bar{v}\frac{\partial \bar{h}}{\partial \bar{y}} - \bar{h}_x \frac{\partial \bar{u}}{\partial \bar{x}} - \bar{h}_y \frac{\partial \bar{u}}{\partial \bar{y}} = \frac{1}{\gamma}\frac{\partial^2 \bar{h}}{\partial \bar{y}^2} \tag{4}$$

$$\frac{\partial \bar{\theta}}{\partial \tau} + \bar{u}\frac{\partial \bar{\theta}}{\partial \bar{x}} + \bar{v}\frac{\partial \bar{\theta}}{\partial \bar{y}} + S_t\bar{u} = \frac{1}{P_r}\frac{\partial^2 \bar{\theta}}{\partial \bar{y}^2} \tag{5}$$

The dimensionalized boundary conditions in which the dimensionless fluid temperature is $\bar{\theta}$ is written as

$$\bar{\theta} = \frac{T_w - T_{\infty,\bar{x}}}{T_w - T_{\infty,0}} = 1 - \frac{T_{\infty,\bar{x}} - T_{\infty,0}}{T_w - T_{\infty,0}} \tag{6}$$

Since $T_{\infty,\bar{x}}$ is a linear function and $\Delta T_0 = T_w - T_{\infty,0}$ ($T_{\infty,0}$ is constant), the dimensionless temperature can be written as

$$\bar{\theta} = 1 - \frac{1}{\Delta T_0}\frac{dT_{\infty,\bar{x}}}{d\bar{x}}\bar{x} = 1 - S_t\bar{x} \tag{7}$$

In linear form, the thermally stratification S_t is considered to be constant but for other variation it may be characterized as a function of $\bar{x}$. Thus the boundary conditions are:

$$\bar{u} = 0, \quad \bar{v} = 0, \quad \bar{h}_y = \bar{h}_x = 0, \quad \bar{\theta} = 1 - S_t\bar{x} \quad at \quad \bar{y} = 0$$
$$\bar{u} \to \bar{U}(\tau), \quad \bar{\theta} \to 0, \quad \bar{\mathrm{h}}_y \to 1 \quad as \quad \bar{y} \to \infty \tag{8}$$

In Eqs. (1)-(5) with boundary conditions in Eq. (8), ξ is magnetic-force parameter, λ is the mixed convection parameter, γ is the magnetic Prandtl number, Pr is the Prandtl parameter, S_t is thermally stratification parameter and H_o is magnetic field intensity along normal to surface.

$$\xi = \frac{\mu {H_0}^2}{\rho {U_\infty}^2}, \qquad P_r = \frac{\nu}{\alpha}, \qquad S_t = \frac{1}{\Delta T_0}\frac{dT_{\infty,\bar{x}}}{d\bar{x}}, \qquad \gamma = \frac{\nu}{\nu_m}, \tag{9}$$
$$\alpha = \frac{\kappa}{\rho C_p}, \qquad \lambda = \frac{G_{r_L}}{{Re_L}^2}, \qquad Re_L = \frac{U_\infty L}{\nu}, \qquad G_{r_L} = \frac{g\beta\Delta T L^3}{\nu^2}$$

Taking $U(\tau) = 1 + \epsilon e^{i\omega\tau}$ is the stream velocity under $|\epsilon| << 1$, where ϵ is presenting oscillating component with small magnitude and frequency parameter ω. The velocity of fluid, the magnetic velocity and fluid temperature components $u, v, h_x,\ h_y$ and θ are in the sum form of steady and unsteady equations

$$\bar{u} = u_s + \epsilon u_t e^{i\omega\tau}, \qquad \bar{v} = v_s + \epsilon v_t e^{i\omega\tau}, \qquad \bar{h}_x = \mathrm{h}_{xs} + \epsilon \mathrm{h}_{xt} e^{i\omega\tau}$$
$$\bar{h}_y = \mathrm{h}_{ys} + \epsilon \mathrm{h}_{yt} e^{i\omega\tau},\ \bar{\theta} = \theta_s + \epsilon\theta_t e^{i\omega\tau} \tag{10}$$

We can substitute dimensionless governing steady and unsteady equations separately by following orders $O(\varepsilon^0)$ and $O(\varepsilon e^{i\omega\tau})$ in Eqs. (1)-(5) with boundary conditions in Eq. (8) by using Eq. (10) in the form:

The steady components of the given Eqs. (1)-(5) with boundary conditions in Eq. (8) are:

$$\frac{\partial u_s}{\partial x} + \frac{\partial v_s}{\partial y} = 0 \tag{11}$$

$$u_s\frac{\partial u_s}{\partial x} + v_s\frac{\partial u_s}{\partial y} = \frac{\partial^2 u_s}{\partial y^2} + \xi\left(h_{xs}\frac{\partial h_{xs}}{\partial x} + h_{ys}\frac{\partial h_{xs}}{\partial y}\right) + \lambda\theta_s sin\alpha \tag{12}$$

$$\frac{\partial h_{xs}}{\partial x} + \frac{\partial h_{ys}}{\partial y} = 0 \tag{13}$$

$$u_s\frac{\partial h_s}{\partial x} + v_s\frac{\partial h_s}{\partial y} - h_{xs}\frac{\partial u_s}{\partial x} - h_{ys}\frac{\partial u_s}{\partial y} = \frac{1}{\gamma}\frac{\partial^2 h_s}{\partial y^2} \tag{14}$$

$$u_s\frac{\partial \theta_s}{\partial x} + v_s\frac{\partial \theta_s}{\partial y} + S_t u_s = \frac{1}{P_r}\frac{\partial^2 \theta_s}{\partial y^2} \tag{15}$$

with appropriate boundary conditions:

$$u_s = v_s = 0, \quad h_{ys} = h_{xs} = 0, \quad \theta_s = 1 - S_t x \quad at \quad y = 0$$
$$u_s \to 1, \quad \theta_s \to 0, \quad h_{ys} \to 1 \quad as \quad y \to \infty \tag{16}$$

By considering the oscillating stokes conditions given in Eq. (17) to separate the unsteady part into real and imaginary parts. Using the Eq. (17), we concluded the separate form of real and imaginary equations:

$$u_t = u_1 + iu_2, \quad v_t = v_1 + iv_2, \quad \theta_t = \theta_1 + i\theta_2, \quad h_{xt} = h_{x1} + ih_{x2}, \quad h_{yt} = h_{y1} + ih_{y2} \tag{17}$$

The real components of the given Eqs. (1)-(5) with boundary conditions in Eq. (8) are:

$$\frac{\partial u_1}{\partial x} + \frac{\partial v_1}{\partial y} = 0 \tag{18}$$

$$-\omega u_2 + u_s \frac{\partial u_1}{\partial x} + u_1 \frac{\partial u_s}{\partial x} + v_s \frac{\partial u_1}{\partial y} + v_1 \frac{\partial u_s}{\partial y} = \frac{\partial^2 u_1}{\partial y^2} + \xi \left(h_{xs} \frac{\partial h_{x1}}{\partial x} + h_{x1} \frac{\partial h_{xs}}{\partial x} + h_{ys} \frac{\partial h_{x1}}{\partial y} + h_{y1} \frac{\partial h_{xs}}{\partial y} \right) + \lambda \theta_1 sin\alpha \tag{19}$$

$$\frac{\partial h_{x1}}{\partial x} + \frac{\partial h_{y1}}{\partial y} = 0 \tag{20}$$

$$-\omega h_2 + u_s \frac{\partial h_1}{\partial x} + u_1 \frac{\partial h_s}{\partial x} + v_s \frac{\partial h_1}{\partial y} + v_1 \frac{\partial h_s}{\partial y} - h_{xs} \frac{\partial u_1}{\partial x} - h_{x1} \frac{\partial u_s}{\partial x} - h_{ys} \frac{\partial u_1}{\partial y} - h_{y1} \frac{\partial u_s}{\partial y} = \frac{1}{\gamma} \frac{\partial^2 h_1}{\partial y^2} \tag{21}$$

$$-\omega \theta_2 + u_s \frac{\partial \theta_1}{\partial x} + u_1 \frac{\partial \theta_s}{\partial x} + v_s \frac{\partial \theta_1}{\partial y} + v_1 \frac{\partial \theta_s}{\partial y} + S_t u_1 = \frac{1}{P_r} \frac{\partial^2 \theta_1}{\partial y^2} \tag{22}$$

along with boundary conditions:

$$u_1 = v_1 = 0, \quad h_{y1} = h_{x1} = 0, \quad \theta_1 = 1 - S_t x \quad at \quad y = 0$$
$$u_1 \to 1, \quad \theta_1 \to 0, \quad h_{y1} \to 1 \quad as \quad y \to \infty \tag{23}$$

The imaginary components of the given Eqs. (1)-(5) with boundary conditions in Eq. (8) are:

$$\frac{\partial u_2}{\partial x} + \frac{\partial v_2}{\partial y} = 0 \tag{24}$$

$$\omega(u_1 - U_o) + u_s \frac{\partial u_2}{\partial x} + u_2 \frac{\partial u_s}{\partial x} + v_s \frac{\partial u_2}{\partial y} + v_2 \frac{\partial u_s}{\partial y} = \frac{\partial^2 u_2}{\partial y^2} + \xi \left(h_{xs} \frac{\partial h_{x2}}{\partial x} + h_{x2} \frac{\partial h_{xs}}{\partial x} + h_{ys} \frac{\partial h_{x2}}{\partial y} + h_{y2} \frac{\partial h_{xs}}{\partial y} \right) + \lambda \theta_2 sin\alpha \tag{25}$$

$$\frac{\partial h_{x2}}{\partial x} + \frac{\partial h_{y2}}{\partial y} = 0 \tag{26}$$

$$\omega h_1 + u_s \frac{\partial h_2}{\partial x} + u_2 \frac{\partial h_s}{\partial x} + v_s \frac{\partial h_2}{\partial y} + v_2 \frac{\partial h_s}{\partial y} - h_{xs} \frac{\partial u_2}{\partial x} - h_{x2} \frac{\partial u_s}{\partial x} - h_{ys} \frac{\partial u_2}{\partial y} - h_{y2} \frac{\partial u_s}{\partial y} = \frac{1}{\gamma} \frac{\partial^2 h_2}{\partial y^2} \tag{27}$$

$$\omega \theta_1 + u_s \frac{\partial \theta_2}{\partial x} + u_2 \frac{\partial \theta_s}{\partial x} + v_s \frac{\partial \theta_2}{\partial y} + v_2 \frac{\partial \theta_s}{\partial y} + S_t u_2 = \frac{1}{P_r} \frac{\partial^2 \theta_2}{\partial y^2} \tag{28}$$

along with boundary conditions:

$$u_2 = v_2 = 0, \quad h_{y2} = h_{x2} = 0, \quad \theta_2 = 0 \quad at \quad y = 0$$
$$u_2 \to 0, \quad \theta_2 \to 0, \quad h_{y2} \to 0 \quad as \quad y \to \infty. \tag{29}$$

3 Computational analysis

The above obtained dimensionless governing steady, real and imaginary coupled equations are discritized numerically by applying finite-difference scheme. Using the Primitive Transformation to obtained primitive form of coupled partial differential equation for further integration. For this purpose, we use the following transformation mentioned in Eq. (30) for steady part to convert into suitable form with both dependent and independent variables as:

$$u_s(x,y) = U_s(X,Y), \quad v_s(x,y) = x^{\frac{-1}{2}}V_s(X,Y), \qquad h_{ys}(x,y) = x^{\frac{-1}{2}}\varphi_{ys}(X,Y),$$

$$h_{xs}(x,y) = \varphi_{xs}(X,Y), \qquad \theta_s(x,y) = \theta_s(X,Y), \qquad Y = x^{\frac{-1}{2}}y, \qquad X = x \tag{30}$$

The primitive form of steady equations in Eqs. (11)-(16), by using Eq. (30), we have

$$X\frac{\partial U_s}{\partial X} - \frac{Y}{2}\frac{\partial U_s}{\partial Y} + \frac{\partial V_s}{\partial Y} = 0 \tag{31}$$

$$XU_s\frac{\partial U_s}{\partial X} + \left[V_s - \frac{Y}{2}U_s\right]\frac{\partial U_s}{\partial Y} = \frac{\partial^2 U_s}{\partial Y^2} + \xi\left[X\varphi_{xs}\frac{\partial \varphi_{xs}}{\partial Y} + \left(\varphi_{ys} - \frac{Y}{2}\varphi_{xs}\right)\frac{\partial \varphi_{xs}}{\partial Y}\right] + \lambda\theta_s sin\alpha \tag{32}$$

$$X\frac{\partial \varphi_{xs}}{\partial X} - \frac{Y}{2}\frac{\partial \varphi x_s}{\partial Y} + \frac{\partial \varphi_{ys}}{\partial Y} = 0 \tag{33}$$

$$XU_s\frac{\partial \varphi_s}{\partial X} + \left[V_s - \frac{Y}{2}U_s\right]\frac{\partial \varphi_s}{\partial Y} - X\varphi_{xs}\frac{\partial U_s}{\partial Y} - \left(\varphi_{ys} - \frac{Y}{2}\varphi_{xs}\right)\frac{\partial U_s}{\partial Y} = \frac{1}{\gamma}\frac{\partial^2 \varphi_s}{\partial Y^2} \tag{34}$$

$$XU_s\frac{\partial \theta_s}{\partial X} + \left[V_s - \frac{Y}{2}U_s\right]\frac{\partial \theta_s}{\partial Y} + S_t XU_s = \frac{1}{P_r}\frac{\partial^2 \theta_s}{\partial Y^2} \tag{35}$$

with boundary conditions as:

$$U_s = V_s = 0, \quad \varphi_{ys} = \varphi_{xs} = 0, \quad \theta_s = 1 - S_t X \quad at \quad Y = 0$$

$$U_s \to 1, \qquad \theta_s \to 0, \qquad \varphi_{ys} \to 1 \quad as \quad Y \to \infty. \tag{36}$$

The primitive form of real equations in Eqs. (18)-(23), by using Eq. (37), we have

$$u_1(x,y) = U_1(X,Y), \quad v_1(x,y) = x^{\frac{-1}{2}}V_1(X,Y), \quad h_{y1}(x,y) = x^{\frac{-1}{2}}\varphi_{y1}(X,Y),$$

$$h_{x1}(x,y) = \varphi_{x1}(X,Y), \quad \theta_1(x,y) = \theta_1(X,Y), \quad Y = x^{\frac{-1}{2}}y, \qquad X = x \tag{37}$$

Using Eq. (37) in Eqs. (18)-(23), the reduced system of primitive equations

$$X\frac{\partial U_1}{\partial X} - \frac{Y}{2}\frac{\partial U_1}{\partial Y} + \frac{\partial V_1}{\partial Y} = 0 \tag{38}$$

$$X\left[U_s\frac{\partial U_1}{\partial X} + U_1\frac{\partial U_s}{\partial X}\right] + \left[V_s - \frac{Y}{2}U_s\right]\frac{\partial U_1}{\partial Y} + \left[V_1 - \frac{Y}{2}U_1\right]\frac{\partial U_s}{\partial Y} - \omega XU_2 = \frac{\partial^2 U_1}{\partial Y^2} +$$
$$\xi\left[X\left(\varphi_{xs}\frac{\partial \varphi_{x1}}{\partial x} + \varphi_{x1}\frac{\partial \varphi_{xs}}{\partial x}\right) + \left(\varphi_{ys} - \frac{Y}{2}\varphi_{xs}\right)\frac{\partial \varphi_{x1}}{\partial Y} + \left(\varphi_{y1} - \frac{Y}{2}\varphi_{x1}\right)\frac{\partial \varphi_{xs}}{\partial Y}\right] + \lambda\theta_1 sin\alpha \tag{39}$$

$$X\frac{\partial \varphi_{x1}}{\partial X} - \frac{Y}{2}\frac{\partial \varphi_{x1}}{\partial Y} + \frac{\partial \varphi_{y1}}{\partial Y} = 0 \tag{40}$$

$$X\left[U_s\frac{\partial \varphi_1}{\partial X} + U_1\frac{\partial \varphi_s}{\partial X}\right] + \left[V_s - \frac{Y}{2}U_s\right]\frac{\partial \varphi_1}{\partial Y} + \left[V_1 - \frac{Y}{2}U_1\right]\frac{\partial \varphi_s}{\partial Y} - \omega X\varphi_2\left[X\left(\varphi_{xs}\frac{\partial U_1}{\partial x} +\right.\right.$$
$$\left.\left.\varphi_{x1}\frac{\partial U_s}{\partial x}\right) + \left(\varphi_{ys} - \frac{Y}{2}\varphi_{xs}\right)\frac{\partial U_1}{\partial Y} + \left(\varphi_{y1} - \frac{Y}{2}\varphi_{x1}\right)\frac{\partial U_s}{\partial Y}\right] = \frac{1}{\gamma}\frac{\partial^2 \varphi_1}{\partial Y^2} \tag{41}$$

$$X\left[U_s\frac{\partial \theta_1}{\partial X} + U_1\frac{\partial \theta_s}{\partial X}\right] + \left[V_s - \frac{Y}{2}U_s\right]\frac{\partial \theta_1}{\partial Y} + \left[V_1 - \frac{Y}{2}U_1\right]\frac{\partial \theta_s}{\partial Y} - \omega X\theta_2 + S_t XU_1 = \frac{1}{P_r}\frac{\partial^2 \theta_1}{\partial Y^2} \tag{42}$$

with boundary conditions as:

$$U_1 = V_1 = 0, \quad \varphi_{y1} = \varphi_{x1} = 0, \quad \theta_1 = 1 - S_t X \ \ at \ \ Y = 0$$
$$U_1 \to 1, \qquad \theta_1 \to 0, \qquad \varphi_{Y1} \to 1 \quad as \ \ Y \to \infty \tag{43}$$

The primitive form of real equations in Eqs. (24)-(29), by using Eq. (44), we have

$$u_2(x,y) = U_2(X,Y), \quad v_2(x,y) = x^{\frac{-1}{2}} V_2(X,Y), \qquad h_{y2}(x,y) = x^{\frac{-1}{2}} \varphi_{y2}(X,Y),$$
$$h_{x2}(x,y) = \varphi_{x2}(X,Y), \qquad \theta_2(x,y) = \theta_2(X,Y), \ \ Y = x^{\frac{-1}{2}} y, \qquad X = x \tag{44}$$

Using Eq. (44) in Eqs. (24)-(29), the reduced system of primitive equations

$$X\frac{\partial U_2}{\partial X} - \frac{Y}{2}\frac{\partial U_2}{\partial Y} + \frac{\partial V_2}{\partial Y} = 0 \tag{45}$$
$$X\left[U_s\frac{\partial U_2}{\partial X} + U_2\frac{\partial U_s}{\partial X}\right] + \left[V_s - \frac{Y}{2}U_s\right]\frac{\partial U_2}{\partial Y} + \left[V_2 - \frac{Y}{2}U_2\right]\frac{\partial U_s}{\partial Y} + \omega X(U_1 - U_o) = \frac{\partial^2 U_2}{\partial Y^2} +$$
$$\xi\left[X\left(\varphi_{xs}\frac{\partial \varphi_{x2}}{\partial x} + \varphi_{x2}\frac{\partial \varphi_{xs}}{\partial x}\right) + \left(\varphi_{ys} - \frac{Y}{2}\varphi_{xs}\right)\frac{\partial \varphi_{x2}}{\partial Y} + \left(\varphi_{y2} - \frac{Y}{2}\varphi_{x2}\right)\frac{\partial \varphi_{xs}}{\partial Y}\right] + \lambda\theta_2 sin\alpha \tag{46}$$
$$X\frac{\partial \varphi_{x1}}{\partial X} - \frac{Y}{2}\frac{\partial \varphi_{x1}}{\partial Y} + \frac{\partial \varphi_{y1}}{\partial Y} = 0 \tag{47}$$
$$X\left[U_s\frac{\partial \varphi_2}{\partial X} + U_2\frac{\partial \varphi_s}{\partial X}\right] + \left[V_s - \frac{Y}{2}U_s\right]\frac{\partial \varphi_2}{\partial Y} + \left[V_2 - \frac{Y}{2}U_2\right]\frac{\partial \varphi_s}{\partial Y} + \omega X\varphi_1 - \left[X\left(\varphi_{xs}\frac{\partial U_2}{\partial x} + \right.\right.$$
$$\left.\left.\varphi_{x2}\frac{\partial U_s}{\partial x}\right) + \left(\varphi_{ys} - \frac{Y}{2}\varphi_{xs}\right)\frac{\partial U_2}{\partial Y} + \left(\varphi_{y2} - \frac{Y}{2}\varphi_{x2}\right)\frac{\partial U_s}{\partial Y}\right] = \frac{1}{\gamma}\frac{\partial^2 \varphi_2}{\partial Y^2} \tag{48}$$
$$X\left[U_s\frac{\partial \theta_2}{\partial X} + U_2\frac{\partial \theta_s}{\partial X}\right] + \left[V_s - \frac{Y}{2}U_s\right]\frac{\partial \theta_2}{\partial Y} + \left[V_2 - \frac{Y}{2}U_2\right]\frac{\partial \theta_s}{\partial Y} + \omega X\theta_1 + S_t X U_2 = \frac{1}{P_r}\frac{\partial^2 \theta_2}{\partial Y^2} \tag{49}$$

with boundary conditions as:

$$U_2 = V_2 = 0, \quad \varphi_{y2} = \varphi_{x2} = 0, \quad \theta_2 = 0 \quad at \quad Y = 0$$
$$U_2 \to 0, \qquad \theta_2 \to 0, \qquad \varphi_{y2} \to 0 \quad as \quad Y \to \infty \tag{50}$$

The primitive form of equations given in Eqs. (31)-(50) is carried out by applying the finite-difference scheme. The numerical results of transformed algebraic expressions with unknown variable U, V, θ and φ which can be solved in tri-diagonal matrix form by using the Gaussian-elimination scheme for these unknown variables. The Eq. (51) addresses the obtained results of oscillating skin friction components τ_w, heat transfer q_w and current density j_w at various stations of non-conducting horizontally cylinder, where A_s, A_t and A_m are amplitudes while, α_s, α_t and α_m are phase angles.

$$\tau_w = \left(\frac{\partial U}{\partial Y}\right)_{y=0} + \varepsilon|A_s|Cos(\omega t + \alpha_s), \ \ q_w = \left(\frac{\partial \theta}{\partial Y}\right)_{y=0} + \varepsilon|A_t|Cos(\omega t + \alpha_t),$$
$$j_w = \left(\frac{\partial \varphi}{\partial Y}\right)_{y=0} + \varepsilon|A_m|Cos(\omega t + \alpha_m) \tag{51}$$

where, $A_s = ({u_1}^2 + {u_2}^2)^{\frac{1}{2}}$, $A_t = \left({\theta_1}^2 + {\theta_2}^2\right)^{\frac{1}{2}}$, $A_m = ({\varphi_{x1}}^2 + {\varphi_{x2}}^2)^{\frac{1}{2}}$,
$\alpha_s = \tan^{-1}\left({u_2}/{u_1}\right)$, $\alpha_t = \tan^{-1}\left({\theta_2}/{\theta_1}\right)$, $\alpha_m = \tan^{-1}\left({\varphi_{x2}}/{\varphi_{x1}}\right)$.

4 Results and discussions

The thermally stratification effects on magnetohydrodynamic mixed convection oscillatory flow around three stations $\alpha = \pi/6, \alpha = \pi/3$ and $\alpha = \pi$ of horizontally non-

conducting circular cylinder has been presented in this work. In given transformed computed analysis, the numerical outcomes for dimensionless primitive formed equations are displayed graphically at given boundary conditions. The emerging parameters, such as thermal stratification parameter S_t, Prandtl number Pr, magnetic force ξ, mixed convection parameter λ and magnetic prandtl number γ on oscillatory stratified flow and heat transfer characteristics are computed in details. The addition of thermal stratification showed a good perfection in oscillatory heat transfer from the surface.

In Fig. 2(a) the velocity plots are shown at different positions for three selected values of stratification parameter S_t. The fluid velocity attained certain height at position $\alpha = \pi/6$ and asymptotically approaches to given boundary condition. Due to thermal stratification, fluid velocity shows good variations at each position and maximum value for $S_t = 0.9$. In Fig. 2(b) temperature profiles decreases at each position with thermally stratification parameter S_t, but increases after a certain distance Y from the cylinder. Since an increase in S_t means decrease in surface temperature or increase in free-stream temperature. The thermal boundary-layer thickness is also decreased due to increase in S_t values and similar behavior at $\alpha = \pi/6$ station. The buoyancy term $(T_w - T_\infty)$ within the boundary layer reduces due to increase in stratification parameter S_t. Fig. 2(c) demonstrates the velocity of magnetic field at three stations $\alpha = \pi/6$, $\alpha = \pi/3$ and $\alpha = \pi$ with stratification S_t and examine a good variations at each position. The magnetic-field effects are observed far from the surface in good form and exact at the surface are zero which yields non-conducting phenomena. Fig. 3(a) presented for velocity profiles at selected values of Pr. The fluid velocity attains maximum value but showed small variations at each position for Pr. The temperature profile behavior for Pr is displayed in Fig. 3(b). The thermal boundary layer thickness is reduced due to increase in Pr. The fluid temperature is decreased with similar behavior at each position due to thermal stratification. In Fig. 3(c), the effect of Pr on magnetic field profiles is plotted against three stations. The magnetic profile increases far from the surface as Pr decreases at $\alpha = \pi/6$ position and showed similar behavior at each station. Due to non-conducting mechanism the magnetic effects are appeared far from the surface and exact at the surface are zero presenting good phenomena. This phenomena is valid because due to Lorentz forces the velocity of fluid decreases and low Prandtl value of fluids possess higher thermal conductivities. Figs. 4(a)-4(c) demonstrate the mixed convection parameter λ effects for fluid velocity, temperature and magnetic velocity at three stations $\alpha = \pi/6$, $\alpha = \pi/3$ and $\alpha = \pi$ with thermal stratification. Fig. 4(a) depicted that fluid velocity attains maximum height at $\alpha = \pi/6$ position for higher values of λ. Velocity plots showed good variations at each position in the existence of thermal stratification and satisfying given boundary conditions. In Fig. 4(b) the fluid temperature decreases as λ increases and good variations for $\alpha = \pi/3, \pi$ stations. It is observed that for $S_t = 0.3$ the values of fluid temperature are obtained negative form within the boundary layer. Due to this reason the temperature difference between the ambient and surface is zero for $S_t = 0.3$. But fluid is coming up to the given boundary condition from below by temperature buoyant force which is less than surface or ambient temperature. Fig. 4(c) is plotted for magnetic field at three selected values of λ. The velocity of magnetic field increases as λ increases at position $\alpha = \pi/6$ and good variations are observed at each position. The

most prominent and favorable position for magnetic-velocity is $\alpha = \pi/6$. Because, larger values of λ correspond to stronger buoyancy forces which leads to increase the acceleration of fluid flow. Due to non-conducting phenomena the magnetic effects are strongly observed far from the surface but exact at the surface are zero for each position.

Figs. 5(a)-5(c) are plotted to represent the numerical results of oscillating skin friction τ_w, fluctuating heat transfer rate q_w and j_w is the current density at selected values of stratification parameter S_t at three stations $\alpha = \pi/6$, $\alpha = \pi/3$ and $\alpha = \pi$ of non-conducting horizontally cylinder. In Fig. 5(a) the oscillations in skin friction are examined at each position but maximum for $S_t = 0.01$ at $\alpha = \pi/3$ position. A significant increase in amplitude of heat transfer is claimed for large values of stratification S_t and good variations at both $\alpha = \pi/3$ and π positions in Fig. 5(b). This is due to fact that amplitude of heat transfer would be boosted significantly if the thermal stratification effect is taken into account. The effect of thermal stratification increases the oscillatory current density at each position and showed maximum amplitude at $\alpha = \pi$ position for lower value of $S_t = 0.01$ in Fig. 5(c). The most favorable position for oscillations is observed at $\alpha = \pi/3$. This phenomena is physically correct due to magnetic force which induced a Lorentz force on viscous incompressible fluids. This force resists the fluid velocity which increase the oscillating skin friction τ_w as well as heat transfer q_w at each position. The Figs. 6(a)-6(c) are plotted for oscillatory behavior at selected values of Prandtl number Pr. The amount of oscillatory τ_w is noted maximum at $\alpha = \pi/3$ and good oscillating behavior is found at each position in Fig. 6(a). The considerable oscillating response is noted in heat transfer for larger value of Pr and highest amplitude is found at π position in Fig. 6(b). Physically, it is claimed that the amplitude of heat transfer increases and thermal boundary layer decreases due to higher value of Pr. The Fig. 6(c) is displayed for oscillating current density with thermal stratification. The similar fluctuating response is observed at $\alpha = \pi$ for each value of Pr. A good amplitude is noted in current density on other both positions for larger Pr. A small fluctuation in heat transfer is examined for lower Pr. The Figs. 7(a)-7(c) are displayed oscillatory mechanism for τ_w, q_w and amplitude of j_w at $\alpha = \pi/6$, $\alpha = \pi/3$ and $\alpha = \pi$ positions for selected values of λ. The amplitude of oscillations in skin friction increases as λ increases in Fig. 7(a). Good oscillations in skin friction are obtained at each position with thermal stratification. The highest range in oscillation for heat transfer is plotted at π position in Fig. 7(b). The most prominent and favorable position for λ is π but similar response is checked on other both positions. The Fig. 7(c) shows highest range in amplitude of current density at $\alpha = \pi$ as λ is increased. This phenomena is valid because the maximum value of λ induced a stronger buoyancy force which leads to increase more fluctuations in fluid flow. It is also clear the skin friction increases due to resistive force which opposes the flow.

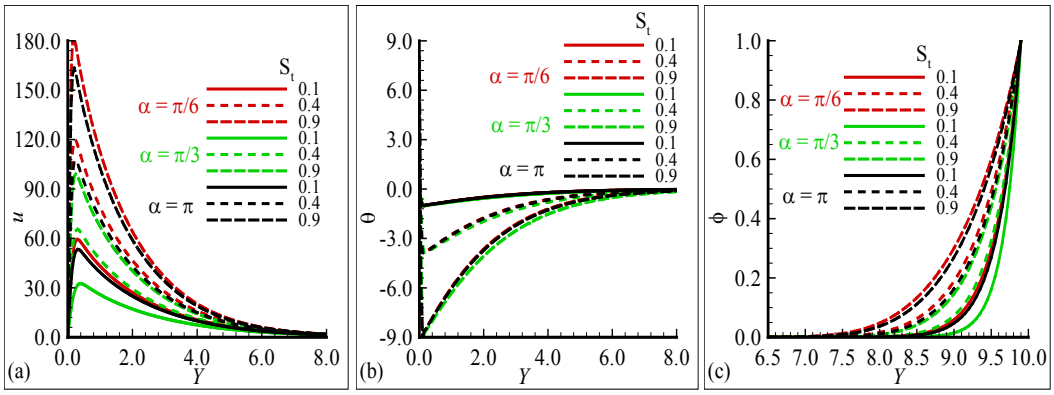

Figure 2: The geometrical profiles for (a) velocity u (b) temperature θ and (c) magnetic field Φ at positions $\alpha = \pi/6$, $\alpha = \pi/3$ and $\alpha = \pi$ with three choice of thermally stratification parameter $S_t = 0.1, 0.4, 0.9$ where others are $\gamma = 0.8$, Pr= 7.0, $\xi = 0.2$ and $\lambda = 6.0$

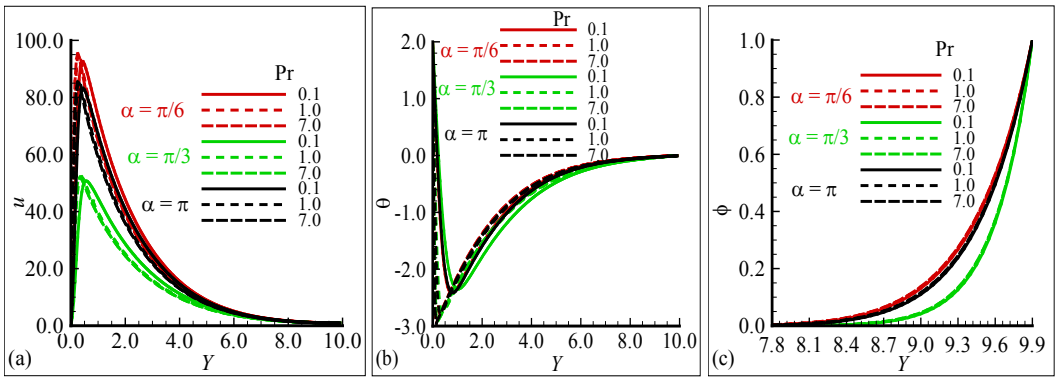

Figure 3: The geometrical profiles for (a) velocity u (b) temperature θ and (c) magnetic field Φ at positions $\alpha = \pi/6$, $\alpha = \pi/3$ and $\alpha = \pi$ at selected values of Pr $= 0.1, 1.0$ and 7.0 while $\gamma = 0.8$, $\xi = 0.8$, $\lambda = 5.1$, and $S_t = 0.3$

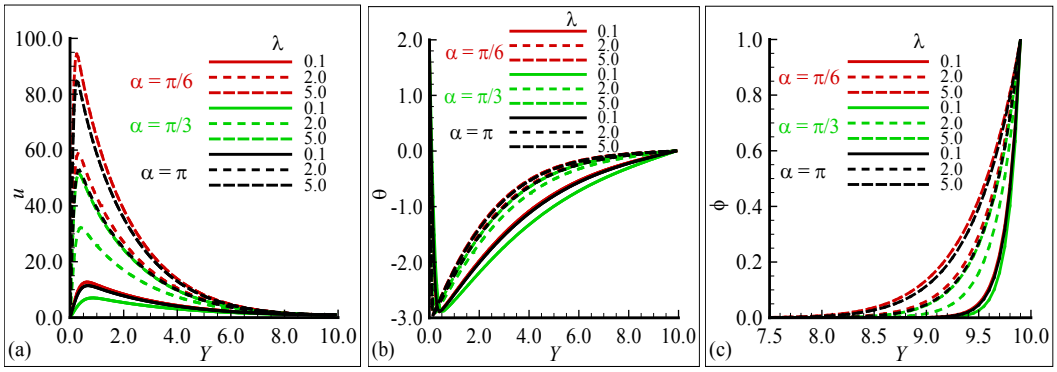

Figure 4: The geometrical profiles for (a) velocity u (b) temperature θ and (c) magnetic field Φ at positions $\alpha = \pi/6$, $\alpha = \pi/3$ and $\alpha = \pi$ at selected values $\lambda = 0.1, 2.0, 5.0$ where others are $S_t = 0.3$, $\xi = 0.7$, Pr= 7.0, and $\gamma = 0.8$

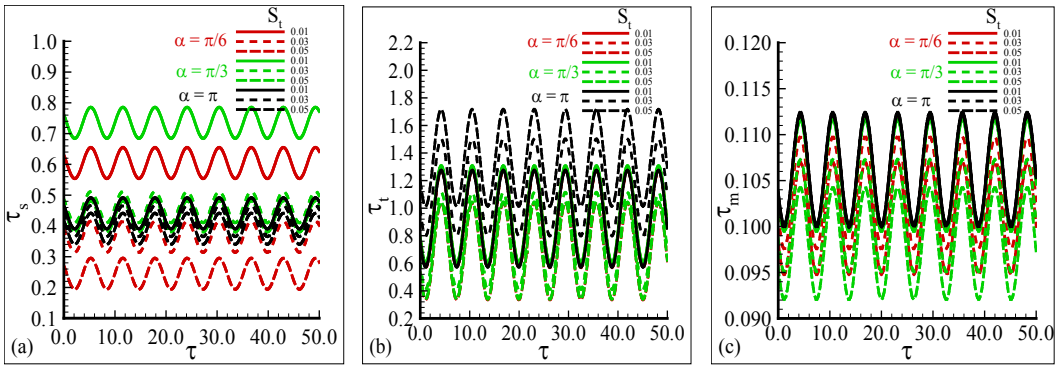

Figure 5: The geometrical profiles of (a) τ_w (b) q_w and (c) j_w at positions $\alpha = \pi/6, \alpha = \pi/3$ and $\alpha = \pi$ with three choice of thermally stratification parameter $S_t = 0.01, 0.03, 0.05$ where other parameters $\gamma = 0.01$, $\xi = 0.2$, Pr= 7.0, and $\lambda = 1.1$

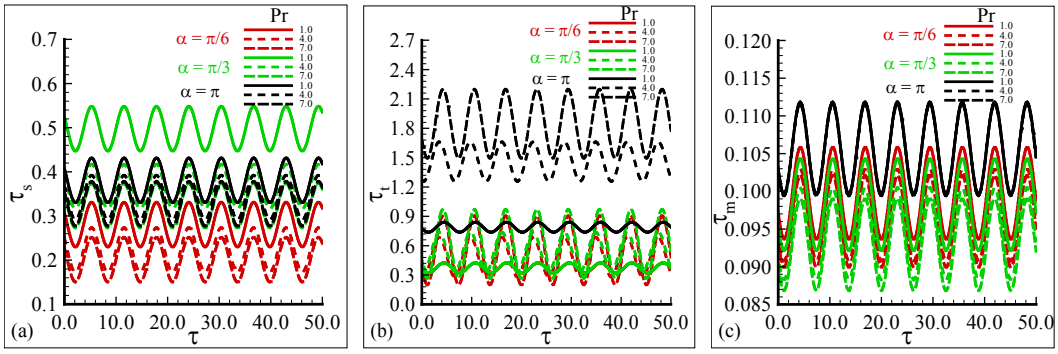

Figure 6: The geometrical profiles of (a) τ_w (b) q_w and (c) j_w at positions $\alpha = \pi/6, \alpha = \pi/3$ and $\alpha = \pi$ with three choice of Pr= 1.0, 4.0, 7.0 where other parameters $\gamma = 0.01$, $\xi = 0.2$, $\lambda = 1.1$, and $S_t = 0.1$

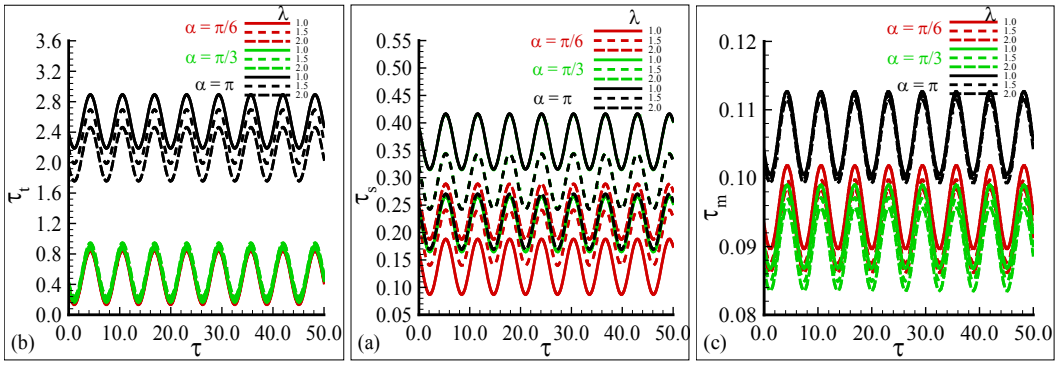

Figure 7: The geometrical profiles of (a) τ_w (b) q_w and (c) j_w at positions $\alpha = \pi/6, \alpha = \pi/3$ and $\alpha = \pi$ with three choice of $\lambda = 1.0, 1.5, 2.0$ where other parameters $\gamma = 0.01$, $\xi = 0.8$, $S_t = 0.15$, and Pr= 7.0 are constant

5 Conclusions

The effects of thermal stratification on magnetohydrodynamic mixed convection oscillatory flow around three stations $\alpha = \pi/6$, $\alpha = \pi/3$ and $\alpha = \pi$ of horizontally non-conducting circular cylinder has been presented in this work. The coupled non-linear PDE's are transformed into suitable form by applying finite-difference scheme with primitive variable formulation to check the accuracy of results. The numerical results of computed analysis at selected values of emerging parameters are displayed graphically around three positions of $\alpha = \pi/6$, $\alpha = \pi/3$ and $\alpha = \pi$ of non-conducting horizontally cylinder. Due to thermal stratification, fluid velocity shows good variations at each position and attains maximum height for $S_t = 0.9$. The fluid temperature is decreased at each position with thermally stratification. Due to non-conducting phenomena the magnetic effects are strongly observed far from the surface but exact at the surface are zero for each position. Since increase in stratification parameter means decrease in surface temperature or increase in free-stream temperature. For Pr the fluid temperature is decreased with similar behavior at each position due to thermal stratification. A significant increase in amplitude of heat transfer is observed for large values of stratification parameter S_t and showed good variations at two stations $\alpha = \pi/3$ and $\alpha = \pi$. The highest range in amplitude is claimed for current density at $\alpha = \pi$ position as λ is increased.

Funding Statement: The authors would like to thank the referees for their valuable comments and suggestions that helped to improve the manuscript. Moreover, the fourth author acknowledges that this publication was supported by Ton Duc Thang University, Vietnam.

Conflicts of Interest: The authors declare no conflicts of interest.

References

Ali, N.; Hussain, I. Y. (2017): Two-dimensional natural convection heat transfer from a heated plate immersed in a thermally stratified medium: numerical and experimental study. *International Journal of Computer Applications*, vol. 179, no. 2, pp. 1-8.

Ashraf, M.; Ahmad, U.; Chamkha, A. J. (2019): Computational analysis of natural convection flow driven along a curved surface in the presence of exothermic catalytic chemical reaction. *Computational Thermal Sciences: An International Journal*, vol. 11, no. 4, pp. 339-351.

Ashraf, M.; Chamakh, A. J.; Iqbal, S.; Ahmad, M. (2016): Effects of temperature dependent viscosity and thermal conductivity on mixed convection flow along a magnetized vertical surface. *International Journal of Numerical Methods for Heat and Fluid Flow*, vol. 26, no. 5, pp. 1580-1592.

Ashraf, M.; Fatima, A. (2018): Numerical simulation of the effect of transient shear stress and rate of heat transfer around different position of sphere in the presence of viscous dissipation. *Journal of Heat Transfer*, vol. 140, no. 6, pp. 1-12.

Ashraf, M.; Fatima, A.; Gorla, R. S. R. (2017): Periodic momentum and thermal boundary layer mixed convection flow around the surface of sphere in the presence of viscous dissipation. *Canadian Journal of Physics*, vol. 95, no. 10, pp. 976-986.

Ashraf, M.; Iqbal, I.; Ahmad, M.; Sultana, N. (2017): Numerical prediction of natural convection flow in the presence of weak magnetic Prandtl number and strong magnetic field with algebraic decay in mainstream velocity. *Advance in Applied Mathematics and Mechanics*, vol. 9, no. 2, pp. 349-361.

Ashraf, M.; Ullah, Z. (2020): Effects of variable density on oscillatory flow around a non-conducting horizontal circular cylinder. *AIP Advances*, vol. 10, no. 1, 015020.

Ashraf, M; Khan, A; Gorla, R. S. R. (2019): Natural convection boundary layer flow of nanofluids around different stations of the sphere and into the plume above the sphere. *Heat Transfer-Asian Research*, vol. 48, no. 3, pp. 1127-1148.

Deka, R. K.; Neog, B. C. (2009): Unsteady natural convection flow past an accelerated vertical plate in a thermally stratified fluid. *Theoretical and Applied Mechanics*, vol. 36, no. 4, pp. 261-274.

Dixit, D. D.; Pattamatta, A. (2020): Effect of uniform external magnetic-field on natural convection heat transfer in a cubical cavity filled with magnetic nano-dispersion. *International Journal of Heat and Mass Transfer*, vol. 146, pp. 118828.

Gireesha, B. J.; Venkatesh, P.; Shashikumar, N. S.; Prasannakumara, B. C. (2017): Boundary layer flow of dusty fluid over a radiating stretching surface embedded in a thermally stratified porous medium in the presence of uniform heat source. *Nonlinear Engineering*, vol. 6, no. 1, pp. 31-41.

Hayat, T.; Asad, S.; Alsaedi, A. (2016): MHD mixed convection flow of burger's fluid in a thermally stratified medium. *Journal of Aerospace Engineering*, vol. 29, no. 6, pp. 1-7.

Hayat, T.; Muhammad, T.; Shehzad, S. A.; Alsaedi, A. (2015): Temperature and concentration stratification effects in mixed convection flow of an Oldroyd-b fluid with thermal radiation and chemical reaction. *PloS One*, vol. 10, no. 6, pp. 1-23.

Hayat, T.; Saeed, Y.; Asad, S.; Alsaedi, A. (2016): Convective heat and mass transfer in flow by an inclined stretching cylinder. *Journal of Molecular Liquids*, vol. 220, pp. 573-580.

Hayat, T.; Waqas, M.; Khan, M. I.; Alsaedi, A. (2016): Analysis of thixotropic nanomaterial in a doubly stratified medium considering magnetic field effects. *International Journal of Heat and Mass Transfer*, vol. 102, pp. 1123-1129.

Hayat, T.; Waqas, M.; Shehzad, S. A.; Alsaedi, A. (2016): Mixed convection flow of a burgers nanofluid in the presence of stratifications and heat generation/absorption. *The European Physical Journal Plus*, vol. 131, pp. 253.

Hussain, I. Y.; Raheem, B. K. (2013): Natural convection heat transfer from a plane wall to thermally stratified porous media. *International Journal of Computer Applications*, vol. 65, no. 1, pp. 42-49.

Ishak, A.; Nazar, R.; Pop, I. (2008): Mixed convection boundary layer flow adjacent to a vertical surface embedded in a stable stratified medium. *International Journal of Heat and Mass Transfer*, vol. 51, no. 13-14, pp. 3693-3695.

Mahmoud, M. A. A.; Waheed, S. E. (2013): Mixed convection flow of a micropolar fluid past a vertical stretching surface in a thermally stratified porous medium with thermal radiation. *Journal of Mechanics*, vol. 29, no. 3, pp. 461-470.

Makinde, O. D.; Reddy, M. G. (2019): MHD peristaltic slip flow of casson fluid and heat transfer in channel filled with a porous medium. *Scientia Iranica*, vol. 26, no. 4, pp. 2342-2355.

Mukhopadhyay, S. (2013): MHD boundary layer flow and heat transfer over an exponentially stretching sheet embedded in a thermally stratified medium. *Alexandria Engineering Journal*, vol. 52, no. 3, pp. 259-265.

Mukhopadhyay, S.; Ishak, A. (2012): Mixed convection flow along a stretching cylinder in a thermally stratified medium. *Journal of Applied Mathematics*, vol. 2012, pp. 491695.

Rehman, K. U.; Malik, M. Y.; Salahuddin, T.; Naseer, M. (2016): Dual stratified mixed convection flow of Eyring-Powell fluid over an inclined stretching cylinder with heat generation/absorption effect. *AIP Advances*, vol. 6, no. 7, 075112.

Saha, S. C.; Hossain, M. A. (2004): Natural convection flow with combined buoyancy effects due to thermal and mass diffusion in a thermally stratified media. *Nonlinear Analysis: Modeling and Control*, vol. 9, no. 1, pp. 89-102.

Saikrishnan, P.; Roy, S.; Takhar, H. S.; Ravindran, R. (2010): Role of thermally stratified medium on a free convection flow from a rotating sphere. *International Journal of Numerical Methods for Heat and Fluid Flow*, vol. 20, no. 1, pp. 96-110.

Ullah, Z.; Ashraf, M.; Rashad, A. M. (2020): Magneto-thermo analysis of oscillatory flow around a non-conducting horizontal circular cylinder. *Journal of Thermal Science and Calorimetry*.

Vasu, B.; Reddy, C. R.; Murthy, P. V. S. N.; Gorla, R. S. R. (2017): Entropy generation analysis in nonlinear convection flow of thermally stratified fluid in saturated porous medium with convective boundary condition. *Journal of Heat Transfer*, vol. 139, no. 9, 091701.

Vyas, A.; Mishra, B.; Srivastava, (2020): A experiments on flow and heat transfer characteristics of a rectangular channel with a built-in adiabatic square cylinder. *International Journal of Heat and Mass Transfer*, vol. 147, pp. 118908.

Yasin, M. H. M.; Arifin, N. M.; Nazar, R.; Ismail, F.; Pop, I. (2013): Mixed convection boundary layer flow embedded in a thermally stratified porous medium saturated by a nanofluid. *Advances in Mechanical Engineering*, vol. 2013, pp. 121943.

Zhang, D. Y.; Yin, T.; Yang, G. B.; Xia, M.; Li, L. D. et al. (2017): Detecting image seam carving with low scaling ratio using multi-scale spatial and spectral entropies. *Journal of Visual Communication and Image Representation*, vol. 48, pp. 281-291.

Zhang, Z.; Li, Y. B.; Wang, C.; Wang, M. Y.; Tu, Y. et al. (2018): An ensemble learning method for wireless multimedia device identification. *Security and Communication Networks*.